



HAL
open science

Silver-based monomer and coordination polymer with organic thiocyanate ligand: Structural, computational and antiproliferative activity study

Nenad R. Filipović, Predrag Ristić, Goran Janjić, Olivera Klisurić, Adrián Puerta, José Padrón, Morgan Donnard, Mihaela Gulea, Tamara Todorović

► To cite this version:

Nenad R. Filipović, Predrag Ristić, Goran Janjić, Olivera Klisurić, Adrián Puerta, et al.. Silver-based monomer and coordination polymer with organic thiocyanate ligand: Structural, computational and antiproliferative activity study. *Polyhedron*, 2019, 173, pp.114132. 10.1016/j.poly.2019.114132 . hal-02319545

HAL Id: hal-02319545

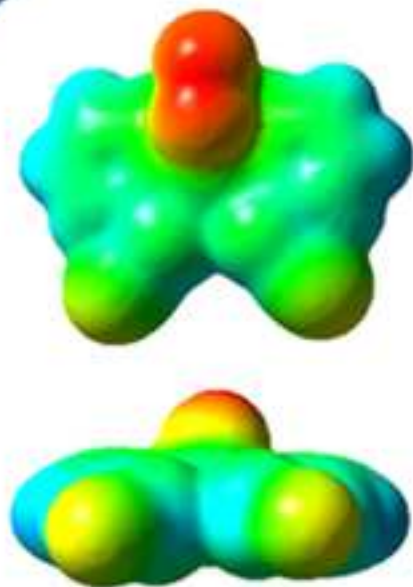
<https://hal.science/hal-02319545>

Submitted on 5 Nov 2020

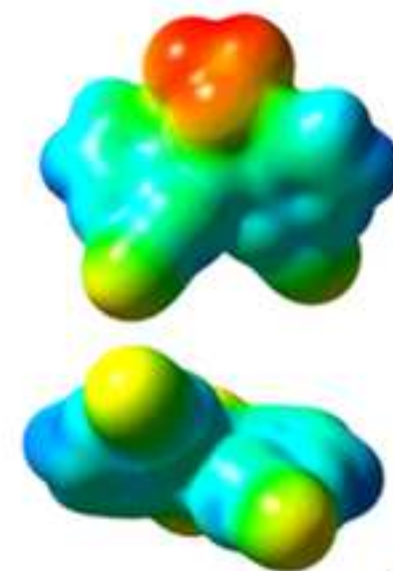
HAL is a multi-disciplinary open access archive for the deposit and dissemination of scientific research documents, whether they are published or not. The documents may come from teaching and research institutions in France or abroad, or from public or private research centers.

L'archive ouverte pluridisciplinaire **HAL**, est destinée au dépôt et à la diffusion de documents scientifiques de niveau recherche, publiés ou non, émanant des établissements d'enseignement et de recherche français ou étrangers, des laboratoires publics ou privés.

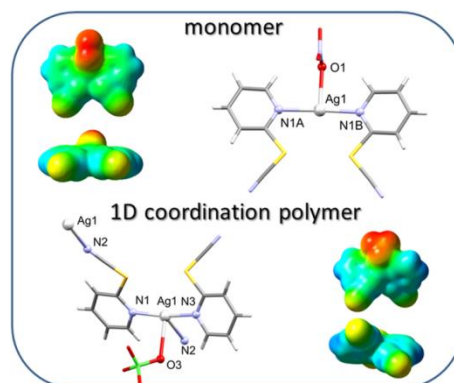
monomer



1D coordination polymer



Graphical Abstract



Analyzed structures of silver-based monomer and coordination polymer with organic thiocyanate represent an example where the nature of (non)coordinated ions were found to have the profound influence on coordination mode of the ligand and consequently crystal packing. The monomer showed an excellent antiproliferative activity in tested human tumor cell lines.

1
2
3
4 **Silver-based monomer and coordination polymer with organic thiocyanate**
5
6
7 **ligand: structural, computational and antiproliferative activity study**
8
9

10 Nenad R. Filipović^a, Predrag Ristić^b, Goran Janjić^c, Olivera Klisurić^d, Adrián Puerta^e,
11
12 José M. Padrón^e, Morgan Donnard^f, Mihaela Gulea^g, Tamara R. Todorović^{b,*}
13
14

15
16
17 *^aFaculty of Agriculture, University of Belgrade, Nemanjina 6, 11000 Belgrade, Serbia;*

18
19 *^bUniversity of Belgrade - Faculty of Chemistry, Studentski trg 12-16, 11000 Belgrade, Serbia;*

20
21
22 *^cInstitute of Chemistry, Technology and Metallurgy, University of Belgrade, Njegoševa 12,*
23
24 *11000 Belgrade, Serbia;*

25
26
27 *^dUniversity of Novi Sad - Faculty of Sciences, Trg Dositeja Obradovića 4, 21000 Novi Sad,*
28
29 *Serbia;*

30
31
32 *^eBioLab, Instituto Universitario de Bio-Orgánica “Antonio González” (IUBO-AG), Centro de*
33
34 *Investigaciones Biomédicas de Canarias (CIBICAN), Universidad de La Laguna, Apartado 456,*
35
36 *E-38071 La Laguna, Spain;*

37
38
39 *^fUniversité de Strasbourg, Université de Haute-Alsace, CNRS, LIMA - UMR 7042, ECPM,*
40
41 *67000 Strasbourg, France*

42
43
44 *^gUniversité de Strasbourg, CNRS, LIT - UMR 7200, Faculty of Pharmacy, 67000 Strasbourg,*
45
46 *France*

47
48
49
50
51
52
53
54 ***Corresponding author: Tamara R. Todorović, PhD, Associate Professor, University of Belgrade**
55
56 **- Faculty of Chemistry, Studentski trg 12-16, 11000 Belgrade, Serbia; E-mail:**
57
58 **tamarat@chem.bg.ac.rs**
59
60

1
2
3
4 **Abstract:**
5

6 The first complexes of 2-pyridylthiocyanate (L) and silver nitrate (**1**) and perchlorate (**2**) were
7 prepared and characterized by a single crystal X-ray analysis. The common structural motif of
8 both **1** and **2** is coordination of two L molecules *via* pyridine nitrogen atom to Ag(I). In order to
9 properly describe the nature of coordinative bonds in **1** and **2**, as well as crystal packings in
10 respective structures, a Quantum Theory of Atoms in Molecule topological analysis was
11 performed. Coordinated nitrate ion provides more electron density to Ag(I) in comparison to
12 perchlorate ion. Additional electron density in the case of **2** was provided by the coordination of
13 third L molecule *via* thiocyanate nitrogen atom resulting in a 1D polymeric structure. Detailed
14 computational analysis of intermolecular interactions, as well analysis of interactions between
15 pyridine ring and –SCN group was performed. Antiproliferative activity of monomeric
16 compound **1** was found to be better than of cisplatin on three out of four studied human cancer
17 cell lines. Docking studies indicate intercalation as a major binding mode of **1** to DNA, while
18 human serum albumin was revealed as possible carrier for distribution of **1** in the blood stream.
19
20
21
22
23
24
25
26
27
28
29
30
31
32
33
34
35
36
37
38
39
40

41 **Keywords:** Silver; organic thiocyanates; coordination polymers; antiproliferative activity;
42
43 docking.
44
45
46
47

48 **Introduction**
49

50 In comparison to the widely used thiocyanate ion as inorganic ligand in metallic
51 complexes (more than 7000 structures referenced in the Cambridge Structural Data base [1],
52 CSD), coordination chemistry of organic thiocyanates [2] (OTCs; R-SCN; R = alkyl, aryl) has
53 been studied in a much lower extend. In the case of Cr, Co, Cd, Mo, Mn, Ag, Pt, Fe as central
54
55
56
57
58
59
60
61
62
63
64
65

1
2
3
4 atoms, OTCs are coordinated *via* nitrogen atom in a simple monodentate fashion, while there are
5
6 only two structures in which nitrogen atom acts as a bridge between metal ions [3]. Among 54
7
8 ligands employed for preparation of OTC-based coordination compounds (OTCCCs) only 9-(2-
9
10 thiocyanatoethyl)adenine possesses additional donor atoms in R group resulted in formation of
11
12 2D coordination polymers (CPs) of corresponding silver(I) and copper(I) complexes [4]. In 14
13
14 structures deposited in the CSD, the coordination of OTCs occurs exclusively *via* nitrogen atom
15
16
17 [1].
18
19
20

21 Among the different families of organometallic complexes, those based on silver as
22
23 metallic center are particularly interesting in terms of therapeutic perspectives. They have found
24
25 applications in a wide scope of medicinal applications such as, non-exhaustively, antiseptics,
26
27 anti-inflammatory or antibacterial agents [5]. More recently such type of complexes has found an
28
29 interest in the field of cancer treatment and interesting data have been reported. Among them
30
31 silver-centered complexes based on thiocyanate anion have given very encouraging results
32
33 against esophageal cancer [6]. Although a large number of silver(I) CPs with diverse topologies
34
35 and dimensionalities are known [7], to the best of our knowledge, there are no reports on 1D and
36
37 3D silver-based CPs with OTC ligands. Neither their synthesis nor their application in medicinal
38
39 chemistry has been investigated so far.
40
41
42
43
44

45 For these reasons, in the present work, we explored coordination ability of a particular
46
47 OTC ligand possessing additional nitrogen donor atom incorporated in a pyridine ring, namely
48
49 2-pyridylthiocyanate (L), toward silver(I) ion in the presence of different anions (*i.e.* nitrate and
50
51 perchlorate). These new organometallic compounds were characterized by a single crystal X-ray
52
53 analysis (SC-XRD). In order to explore the anion effect on the structure of these complexes,
54
55 topological analyses of the electron density were performed. Energy distribution of
56
57
58
59
60
61
62
63
64
65

1
2
3
4 intermolecular interactions was calculated for both species, monomeric nitrate-based compound
5
6 (1) and 1D polymeric perchlorate-based compound (2). The maps of calculated electrostatic
7
8 potential for both compounds were used to get insight into intermolecular interactions
9
10 responsible for formation of respective crystal packings. In order to describe geometry of the
11
12 dominant intermolecular interactions, a statistical analysis of crystal structures extracted from the
13
14 CSD was performed. As mentioned previously, such kind of silver-based complexes are
15
16 promising as antiproliferative agents. Thus, a screening of antiproliferative activity of
17
18 monomeric complex 1 was performed on a panel of four human solid tumor cell lines, while
19
20 docking studies were performed in order to test if DNA is a possible target for 1, and whether
21
22 human serum albumin can be its carrier *via* bloodstream.
23
24
25
26
27
28
29
30

31 **Experimental**

32 ***General remarks***

33
34 Silver nitrate (99%) and silver perchlorate (99%) were obtained from Merck. Reaction-solvents
35
36 were bought anhydrous from Aldrich and used as purchased. Crude ligand was purified by flash
37
38 column chromatography on Merck silica gel Si 60 (40-63 μm). Analytical TLC was carried out
39
40 on Merck aluminum sheets silica gel 60 F254. Elemental analyses (C, H, N) were performed by
41
42 standard micro-methods using the ELEMENTARVario ELIII C.H.N.S@O analyzer. Infra-red
43
44 (IR) spectra were recorded on a Thermo Scientific Nicolet 6700 FT-IR spectrometer by the
45
46 Attenuated Total Reflection (ATR) technique in the region 4000–400 cm^{-1} . Abbreviations used
47
48 for IR spectra: vs, very strong; s, strong; m, medium; w, weak. ^1H NMR spectra were recorded
49
50 at 400 MHz using the residual solvent signal as internal reference (CDCl_3 , 7.26 ppm). Chemical
51
52 shifts are quoted in ppm, coupling constants (J) are given in Hz. The following abbreviations are
53
54
55
56
57
58
59
60
61
62
63
64
65

1
2
3
4 used to describe peak patterns when appropriate: s (singlet), d (doublet), t (triplet), q (quartet),
5
6 quint (quintuplet), hext (hextuplet), hept (heptuplet), m (multiplet) and b (broad). ¹³C NMR
7
8 spectra were recorded at 100 MHz at ambient temperature in CDCl₃ with δ (CDCl₃) at 77.23
9
10 ppm as internal standard.
11
12
13
14

15 16 ***Synthesis of 2-pyridyl thiocyanate ligand (L) [8]*** 17

18
19 In a round bottom flask, 1,2-di(pyridin-2-yl)disulfane (110 mg, 0.5 equiv., 0.5 mmol),
20
21 acetonitrile (3 mL) and tetramethylethylenediamine (232 mg, 2 equiv, 2mmol) were mixed
22
23 together. Then CuCN (179 mg, 2 equiv, 2 mmol) was added and the mixture was let to stir for 18
24
25 h in an open vessel. After a short filtration over Celite[®] that was rinsed thrice with AcOEt (3×3
26
27 mL), the crude mixture was concentrated under vacuum and purified by flash column
28
29 chromatography (heptane/ethyl acetate 90/10) to afford the targeted thiocyanate as a brown oil
30
31 (76%, 104 mg).
32
33

34
35
36 ¹H NMR (400 MHz, CDCl₃) δ 7.26-7.54 (m, 1H), 7.61 (d, *J* = 8.1 Hz, 1H), 7.77 (dt, *J* = 1.8, 7.8
37
38 Hz, 1H), 8.52 (d, *J* = 4.8 Hz, 1H). ¹³C NMR (100.6 MHz, CDCl₃) δ 109.0 (CN), 122.1 (CH),
39
40 122.8 (CH), 138.5 (CH), 150.1 (Cq), 150.6 (CH).
41
42
43
44

45 46 ***Synthesis of [Ag(NO₃)(L)₂] (1) and [Ag(ClO₄)(L)₂]_n (2)*** 47

48
49 Both complexes were synthesized according to a general procedure: into the solution of
50
51 0.184 mmol of corresponding metal salt (AgNO₃, 31.0 mg; AgClO₄, 41.0 mg) in H₂O (10 mL), a
52
53 solution of L (50 mg, 0.367 mmol) in EtOH (10 ml) was added. The reaction mixture was
54
55 refluxed for 1 h and cooled to ambient temperature. Warning: perchlorate salt must be handled
56
57 with caution. Anal. Calcd. for C₁₂H₈AgN₅O₃S₂ (%): C, 32.59; H, 1.82; N, 15.84; S, 14.50.
58
59
60
61
62
63
64
65

1
2
3
4 Found: C, 32.74; H, 1.91; N, 15.99; S, 14.63. Anal. Calcd. for C₁₂H₈AgClN₄O₄S₂ (%): C, 30.05;
5
6 H, 1.68; N, 11.68; S, 13.37. Found: C, 30.17; H, 1.75; N, 11.82; S, 13.51.
7
8

9 **1:** Yield 58 mg (72%); IR (ATR, cm⁻¹): 3099(w), 3054(w), 2361(w), 2336(w), 2163(m), 1583(s),
10
11 1562(s), 1449(vs), 1424(vs), 1397(vs), 1306(vs), 1136(s), 1084(m), 1046(m), 1004(m), 883(w),
12
13 760(s), 723(w), 690(w).
14
15

16 **2:** Yield 52 mg (59%); IR (ATR, cm⁻¹): 3100(w), 3060(w), 2168(m), 1585(s), 1563(m), 1454(s),
17
18 1427(s), 1293(w), 1083(vs), 775(m), 721(w), 619(s).
19
20
21
22

23 *X-ray crystallography*

24
25
26 The diffraction data for **1** was collected at room temperature on Rigaku (Oxford
27
28 Diffraction) Gemini S diffractometer using program package CrysAlis CCD [9] with graphite-
29
30 monochromated MoK α ($\lambda = 0.71071$ Å). The data reduction was performed with program
31
32 package CrysAlis RED [9]. The space group determinations were based on an analysis of the
33
34 Laue class and the systematically absent reflections. Collected data were corrected for absorption
35
36 effects by using Analytical numeric absorption correction applying a multifaceted crystal model
37
38 [9].
39
40
41
42

43 The diffraction data for **2** was collected at 173 K on Bruker APEX-II CCD diffractometer
44
45 using program package Bruker APEX2 [10] with triumph-monochromated MoK α ($\lambda = 0.71071$
46
47 Å). The data reduction was performed with program package Bruker SAINT [10]. The space
48
49 group determinations were based on an analysis of the Laue class and the systematically absent
50
51 reflections. Collected data were corrected for absorption effects by using Multi-scan absorption
52
53 correction [11].
54
55
56
57
58
59
60
61
62
63
64
65

1
2
3
4 The structures were solved by direct methods using SHELXT [12]. The structures were
5
6 refined by full-matrix least-squares procedures on F^2 using SHELXL-2014/6 program [12]. For
7
8 both compounds non-hydrogen atoms were refined anisotropically, the CH hydrogen atoms were
9
10 included on calculated positions riding on their attached atoms with fixed distances of 0.93 Å.
11
12 All calculations were performed using PLATON [13] implemented in the WINGX [14] system
13
14 of programs. MERCURY [15] was employed for molecular graphics. The crystal data and
15
16 refinement parameters are summarized in Table 1.
17
18
19
20
21
22
23
24
25
26
27
28
29
30
31
32
33
34
35
36
37
38
39
40
41
42
43
44
45
46
47
48
49
50
51
52
53
54
55
56
57
58
59
60
61
62
63
64
65

Table 1. Crystallographic data and refinement parameters for **1** and **2**

	1	2
Chemical formula	C ₁₂ H ₈ AgN ₅ O ₃ S ₂	C ₁₂ H ₈ AgClN ₄ O ₄ S ₂
M_r	442.22	479.66
Temperature (K)	293(2)	173(2)
Crystal system	Orthorhombic	Triclinic
Space group	<i>Pbc</i> a	<i>P</i> -1
<i>a</i> (Å)	13.8940(9)	7.7822(3)
<i>b</i> (Å)	9.2116(3)	8.2177(3)
<i>c</i> (Å)	24.2131(8)	14.1789(5)
α (°)	90	104.7850(10)
β (°)	90	91.7410(10)
γ (°)	90	112.0350(10)
ρ_{cal} (Mg/m ³)	1.896	1.980
<i>V</i> (Å ³)	3098.9(2)	804.61(5)
<i>Z</i>	8	2
μ (mm ⁻¹)	1.591	1.704
F(000)	1744	472
Crystal size (mm)	0.804×0.188×0.089	0.250×0.200×0.180
Completeness to $\theta = 25^\circ$	99.9%	99.8%
Absorption correction	Analytical	Multi-scan
T_{min}, T_{max}	0.755, 0.875	0.988, 1.000
Reflections collected	7510	20903
Independent reflections	2719 [<i>R</i> (int) = 0.0220]	5566 [<i>R</i> (int) = 0.0203]
θ values (°)	$\theta_{max} = 24.996, \theta_{min} = 2.783$	$\theta_{max} = 31.992, \theta_{min} = 1.500$
<i>R</i> [$F^2 > 2\sigma(F^2)$], <i>wR</i> 2	0.0347, 0.0674	0.0251, 0.0593
<i>R</i> [<i>all data</i>], <i>wR</i> 2	0.0488, 0.0726	0.0314, 0.0617
Goodness-of-fit (<i>S</i>)	1.128	1.034
No. of parameters	208	217
No. of restraints	0	0
$\Delta\rho_{max}, \Delta\rho_{min}$ (eÅ ⁻³)	0.568, -0.373	0.810, -0.779

Computational methods

To describe the crystal packing within analysed structures, quantum-chemical calculations were performed to estimate the strength of interactions between the corresponding Ag complexes. Calculations were performed in Gaussian09 program [16], using wb97xd functional and def2tzvp basis set.

The electron density for Quantum Theory of Atoms in Molecule (QTAIM) topological analysis [17] was obtained from wb97xd/def2tzvp calculation on the geometries of Ag complexes from crystal structures. QTAIM analysis on electron density topology was done with MultiWfn program [18], while the NCI index and reduced density gradient were calculated with NCIPLOT program [19, 20].

For docking studies, the structure of **1** was optimized at wb97xd/def2tzvp level. Merz–Kollman atomic charges were calculated at same level, according to the scheme via the RESP procedure [21]. Crystal structures of DNA (pdb code: 1BNA) [22] and HSA (pdb code: 1BJ5) [23] were extracted from Protein Data Bank and used for docking study as targets for tested compounds. The structure of DNA represents synthetic double stranded dodecamer d(CpGpCpGpApApTpTpCpGpCpG) with more than one complete turn of right-handed B helix and without DNA intercalation gap. The preparation of DNA and HSA structures have been carried out using AutoDock 4.2 software program [24], and includes the adding of hydrogen atoms and removing other ligands and water molecules from the crystal structures. In order to generate grid and docking parameter files in AutoDockTools program [24] the optimized structures of tested compounds and structures of DNA and HSA were used. The structure of DNA (or HSA) was considered as rigid while coordination bonds of metal complexes were allowed to rotate freely. To accommodate tested compounds during docking study, a grid box,

1
2
3
4 containing the whole DNA (or protein), was used. The virtual screening used Lamarckian
5
6 genetic algorithm as the search method and 100 runs for each docking screen. Discovery Studio
7
8 (BIOVIA Software product) [25] was used to analyse and visualize the results of docking
9
10 studies.
11
12
13
14

15 16 ***CSD search*** 17

18
19 In order to describe the geometry of π - π interactions between SCN group and π -system of
20
21 pyridine ring, the search of CSD was performed. The description of interactions is based on
22
23 statistical analysis of crystal structures extracted from the CSD (version 5.40) [26]. The search of
24
25 CSD was performed using the ConQuest program (version 1.23) [27] to extract all structures
26
27 containing the interacting groups and structures that satisfy the following criteria: (a) no polymer
28
29 structures, (b) no powder structures, (d) crystallographic R factor of <10%, (c) error-free
30
31 coordinates according to the criteria used in the CSD, (e) hydrogen-atom positions that were
32
33 normalized by using the CSD default X-H bond lengths (O-H = 0.983 Å; C-H = 1.083 Å, and
34
35 N-H = 1.009 Å).
36
37
38
39
40
41
42

43 44 ***In vitro antiproliferative activity*** 45

46 The antiproliferative activity of the compounds was studied using our implementation of
47
48 the National Cancer Institute (USA) protocol [28] against human solid tumor cell lines: HBL-
49
50 100 (breast) and HeLa (cervix) as drug sensitive lines, as well as T-47D (breast) and WiDr
51
52 (colon) as drug resistant lines. Cells were inoculated at densities of 2 500 (HBL-100 and HeLa)
53
54 and 5 000 (T-47D and WiDr) cells per well, in a final volume of 100 μ L, based on their doubling
55
56 times. The ligand and complex **1** were initially dissolved in DMSO at 40 mM and tested in
57
58
59
60
61
62
63
64
65

1
2
3
4 triplicate at different dilutions in the range of 1 to 100 μM . A final concentration of DMSO in
5
6 each sample never exciding 0.25% (v/v). Cisplatin, 5-fluorouracil (5-FU) and silver nitrate were
7
8 dissolved in phosphate buffer solution (PBS) while further dilutions have been made in a culture
9
10 medium. Control cells were exposed to an equivalent concentration of DMSO (0.25% v/v,
11
12 negative control). The drug treatment started on day 1 after plating. Drug incubation times were
13
14 48 h, after which cells were precipitated with 25 μL ice-cold trichloroacetic acid (50% w/v) and
15
16 fixed for 60 min at 4 $^{\circ}\text{C}$. Then the sulforhodamine B (SRB) assay was performed [28]. The
17
18 optical density (OD) of each well was measured at 530 nm, using BioTek's PowerWave XS
19
20 Absorbance Microplate Reader. Values were corrected for background OD from wells only
21
22 containing medium. The results are expressed as GI_{50} values (concentration of the tested
23
24 substance that produces 50% growth inhibition).
25
26
27
28
29
30
31
32

33 **Results and discussion**

34 ***Synthesis and characterization***

35
36 Silver-based complexes **1** and **2** were obtained by direct reaction of the ligand *L* and
37
38 corresponding silver(I) salt. Single crystals of both complexes were separated from the mother
39
40 liquor by filtration after several days as colorless prismatic crystals in satisfactory yield.
41
42
43
44

45 Elemental analysis results are in agreement with proposed general formulas.
46
47

48 In the IR spectrum of *L*, characteristic vibration of thiocyanate group $\nu(\text{SC}\equiv\text{N})$, as a band
49
50 of medium intensity was observed at 2162 cm^{-1} . The most intense bands in the spectrum (1570.0
51
52 and 1420.8 cm^{-1}) originate from over tones of pyridine $\delta(\text{C}=\text{N})$ vibration [29]. Almost no shift of
53
54 $\nu(\text{SC}\equiv\text{N})$ in the IR spectrum of **1** (2163 cm^{-1}) indicates lack of thiocyanate group coordination.
55
56
57
58 Contrary, a shift of $\nu(\text{SC}\equiv\text{N})$ to a higher wave number (2168 cm^{-1}) in the IR spectrum of **2**
59
60
61
62
63
64
65

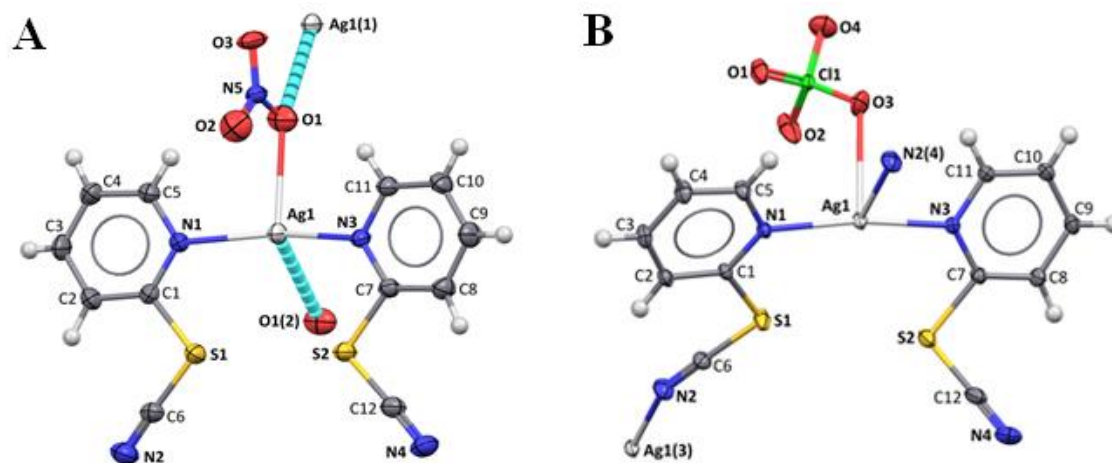
1
2
3
4 indicates coordination of thiocyanate group to silver(I) in this complex. In the IR spectra of both,
5
6
7 **1** and **2**, there are shifts of over tones of pyridine $\delta(\text{C}=\text{N})$ vibrations (1582 and 1423 cm^{-1} in **1**;
8
9 1585 and 1427 cm^{-1} in **2**). This is indication of coordination of pyridine nitrogen atom. In the
10
11 case of **1**, two vibrations originating from nitrate group were observed, while in the IR spectrum
12
13 of **2**, the strongest vibration was assigned to vibration of perchlorate ion [30].
14
15
16
17
18

19 *Description of molecular structures*

20
21 ORTEP drawings of the molecular structures of **1** and **2** are depicted in Figure 1, while
22
23 selected bond distances and bond angles are given in Table 2. Geometry of Ag(I) in **1** is
24
25 deformed T-shaped, where two L molecules are coordinated *via* pyridine nitrogen atom and third
26
27 coordination site is occupied by one oxygen atom (O1) from nitrate. However, taking into
28
29 account the distance between Ag1 and O1(2) atom ($2: \frac{1}{2}-x, -\frac{1}{2}-y, z$) from another nitrate ion
30
31 (2.957 \AA), the coordination number of Ag(I) in **1** can be described also as 3+1 (Figure 1A;
32
33 additional bonds are shown in light blue). Oxygen atom O1 forms unsymmetrical bridge between
34
35 two Ag(I) ions, thus due to this additional weak coordination an infinite 1D chains are formed
36
37 along *b*-axis. The main geometrical features reported in Table 2 show that geometry around
38
39 Ag(I) in **1** is slightly distorted, but nevertheless pyridine rings from two coordinated L ligands
40
41 are almost perfectly planar (the angle between pyridine ring planes is $9.67(14)^\circ$).
42
43
44
45
46
47

48 On the other hand, in **2** Ag(I) ion has coordination number four (Figure 1B) with seesaw
49
50 geometry and Ag1–O3 distance of $2.669(2)\text{ \AA}$. In the inner sphere of the complex two L are
51
52 coordinated *via* pyridine nitrogen atoms, third site is occupied by oxygen atom O3 from
53
54 perchlorate ion, while fourth coordination site is occupied by nitrogen atom N2(4) ($4: x, y-1, z$)
55
56
57
58
59
60
61
62
63
64
65

1
2
3
4 of thiocyanate group from neighboring ligand. The angle between pyridine ring planes in **2** is
5
6
7 23.61(17)°. Complex **2** represents 1D CP, where infinite chains are parallel to *b*-axis.
8
9



29 **Figure 1.** ORTEP drawings of the molecular structures of **1** (A) and **2** (B) with labeling of non-H
30 atoms. Displacement ellipsoids are shown at the 30% probability level and H atoms are drawn as
31 spheres of arbitrary radii. Symmetry codes: (1) $\frac{1}{2}-x, \frac{1}{2}+y, z$; (2) $\frac{1}{2}-x, -\frac{1}{2}-y, z$; (3) $x, y+1, z$;
32
33
34
35
36
37 (4) $x, y-1, z$.
38
39
40

41 By comparing the values of respective bond lengths and angles in **1** and **2** (Table 2) it can be
42 concluded that differences are small and are at the margins of statistical significance.
43
44

45 Although nitrate and perchlorate ions do form complexes with metal cations, the
46 tendency of these ions to coordinate is less than for other common ions. XRD analysis for **1** and
47
48
49
50
51
52
53
54
55
56
57
58
59
60
61
62
63
64
65

2 showed that respective ions are coordinated to Ag(I). In order to check the propensity of perchlorate and nitrate towards coordination to silver(I) a CSD survey has been performed (*vide infra*).

Table 2. Selected bond lengths (Å) and angles (°).

1		2	
Bonds (Å)			
Ag1–N1	2.262(3)	Ag1–N1	2.1887(14)
Ag1–N3	2.254(3)	Ag1–N3	2.1871(14)
Ag1–O1	2.602(3)	Ag1–O3	2.669(2)
Ag1–O1 ²	2.771	N2–Ag1 ³	2.5834(16)
S1–C1	1.779(4)	S1–C1	1.7801(18)
S1–C6	1.683(4)	S1–C6	1.6891(18)
S2–C7	1.777(3)	S2–C7	1.7822(17)
S2–C12	1.680(4)	S2–C12	1.678(3)
Angles (°)			
N3–Ag1–N1	159.01(11)	N3–Ag1–N1	170.43(5)
C1–N1–Ag1	124.7(2)	C1–N1–Ag1	125.05(11)
C5–N1–Ag1	118.3(2)	C5–N1–Ag1	117.76(10)
C7–N3–Ag1	126.2(2)	C7–N3–Ag1	125.24(11)
C11–N3–Ag1	117.0(2)	C11–N3–Ag1	117.46(12)
N1–C1–S1	110.5(3)	N1–C1–S1	110.71(12)
C1–S1–C6	100.64(18)	C1–S1–C6	100.57(9)
C7–S2–C12	101.32(18)	C7–S2–C12	99.11(9)
N3–C7–S2	110.4(3)	N3–C7–S2	112.53(12)

Symmetry codes: (2): $\frac{1}{2}-x, -\frac{1}{2}-y, z$; (3): $x, y+1, z$.

Coordination ability of nitrate and perchlorate to Ag(I) – CSD survey

By analysis of the crystal structures extracted from the CSD, in which the oxygen atom of nitrate ion is simultaneously coordinated to two Ag(I) ions (Figure 2A), it was shown that the values of angle between Ag–O bonds (Ag–O–Ag angle) are in the range from 70 to 160°, with the maximum at 100–120° (Figure 2B). The lengths of Ag–O bonds (d_1 and d_2) are mainly in the range from 2.3 to 2.6 Å (distribution of d parameter, Figure 2C). The difference of d_1 and d_2 distances (Δd parameter, $\Delta d = |d_1 - d_2|$) is not significantly large, because in the most of the structures Δd values are lower than 0.1 Å (Figure 2D).

In the crystal structures in which perchlorate ion is monodentately coordinated to Ag(I) (Figure 2A), lengths of Ag–O bonds are mainly in the range from 2.4 to 2.7 Å (distribution of d parameter, Figure 2E), while values of Ag–O–Cl angles are in the range from 90 to 170°, with the maximum at 100–120° (Figure 2F).

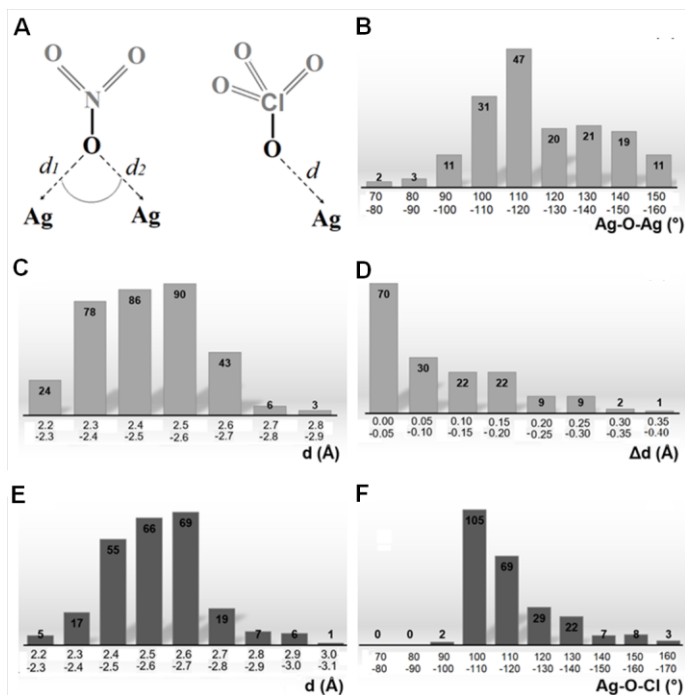


Figure 2. The distribution of parameters describing the geometry of coordination of an oxygen atom from nitrate or perchlorate ligands to Ag(I) ions in the crystal structures extracted from the CSD.

In the crystal structure of **1**, two Ag(I) ions are located close to nitrate oxygen atom O1 (d distances of 2.602 and 2.771 Å). However, the length of the longer interaction is outside the range corresponding to the maximum for distribution of d parameter (Figure 2C), while the difference in bond lengths (Δd) is greater than 0.1 Å. On the other hand, the length of the Ag–O bond in **2** (2.669 Å) is in the range corresponding to the maximum for distribution of d parameter (Figure 2E).

From the crystallographic point of view, bond lengths and angles are only derived quantities, resulting from the atomic positions described as fraction coordinates. In general SHELX program treats a distance between two non-hydrogen atoms as a bond if the distance is

1
2
3
4 less than $r_1 + r_2 + 0.5 \text{ \AA}$, where r_1 and r_2 are the covalent radii of the atoms in question [31].
5
6
7 ”The covalent radii stored in the program are based on experience rather than taken from a
8
9 specific source(s), and are deliberately overestimated for elements which tend to have variable
10
11 coordination numbers so that 'bonds' are no missed, at the cost of generating the occasional 'non-
12
13 bond” [31]. Additionally, bond lengths determined by XRD analysis are distances between
14
15 electron density maxima and not between true positions of the nuclei. However, for the structural
16
17 chemistry, bond distances and angles are the most important molecular characteristics aimed at.
18
19 In order to properly describe the nature of Ag–O bonds in **1** and **2**, as well as crystal packing in
20
21 respective structures, QTAIM topological analysis was made.
22
23
24
25
26
27

28 *QTAIM topological analysis*

29
30
31 QTAIM analysis of wave functions of Ag(I) complexes **1** and **2** has shown the existence
32
33 of five critical points between Ag and O atoms, corresponding to bond critical points (3,–1).
34
35
36 Properties of electron density calculated at these critical points are shown in Table 3.
37
38
39
40
41
42
43
44
45
46
47
48
49
50
51
52
53
54
55
56
57
58
59
60
61
62
63
64
65

Table 3. Properties of electron density calculated at Ag–O bond critical point (3,–1) for **1** and **2** with QTAIM method; strength of bond (d), the electron density ($\rho(r)$), the Laplacian of electron density ($\nabla^2\rho(r)$), total electron energy density (H(r)), the ratio of potential (V(r)) and kinetic (G(r)) electron energy density (k(r)).

Complex	d (Å)	$\rho(r)$ (au)	$\nabla^2\rho(r)$ (au)	H (au)	V(r) (au)	G(r) (au)	k(r)
1							
Ag1···O1	2.602	0.0294	0.1111	–0.0014	–0.0307	0.0293	–1.0478
Ag1···O2	2.952	0.0148	0.0545	0.0010	–0.0117	0.0127	–0.9213
Ag1···O1(2) ^a	2.771	0.0214	0.0750	0.0002	–0.0192	0.0193	–0.9948
Ag1···O2(2)	2.957	0.0144	0.0507	0.0008	–0.0111	0.0119	–0.9328
2							
Ag1···O3	2.669	0.0241	0.0936	–0.0003	–0.0240	0.0237	–1.0127

^aSymmetry code (2): $\frac{1}{2}-x, -\frac{1}{2}-y, z$

The $\rho(r)$ parameter, as an indicator of the bond strength, shows a stronger interaction between Ag1 and O1 atoms of **1** than other Ag···O pairs (Ag1···O1 bond lies in the same plane with two coordinative Ag–N bonds). The positive $\nabla^2\rho(r)$ values indicate the ionic nature of these Ag···O interactions, while the negative value of H(r) parameter suggests a covalent character of Ag1···O1 interaction. Therefore, all Ag···O interactions in **1** can be considered as interactions with ionic character, except the Ag1···O1 interaction that has partial covalent characters. Also, the value of $|k(r)| > 1$ indicates the covalent character of Ag1···O1 interaction.

The $\nabla^2\rho(r)$ parameter for Ag1···O1 interaction in **1** is slightly more positive than $\nabla^2\rho(r)$ parameter for Ag1···O3 interaction in **2**, indicating a more ionic nature of this interaction in **1**. On the other hand, the H(r) parameter for Ag1···O3 bond is less negative than the H(r) parameter for

1
2
3
4 Ag1...O1 bond, suggesting a more covalent nature to the latter. Also, the $|k(r)|$ value of Ag1...O1
5
6 bond is higher than that of Ag1...O3 bond, which also means that this type of interaction has the
7
8 more covalent nature in **1**.
9

10
11 Based on the results of QTAIM analysis, it can be assumed that partial covalent character
12
13 of Ag1...O1 bond reduces the ability of Ag ion in **1** for building additional coordinative bonds.
14
15 The Ag-O3 bond in **2** has ionic character, hence, Ag ion builds the additional Ag-N bond with
16
17 SCN group, in addition to Ag-N bonds with pyridine nitrogen atoms.
18
19
20
21
22

23 ***Energy distribution of intermolecular interactions***

24
25
26 Optimized structures of **1** and **2** are given in Figure 3. In the optimized structure of **1**, Ag
27
28 ion has coordination number four and deformed tetrahedral geometry with Ag-O bonds (2.45
29
30 and 2.49 Å) longer than Ag-N (both 2.20 Å). However, in this complex *ortho* C-H bonds from
31
32 two L molecules form bifurcated C-H/O interactions with the same ligating O atom of nitrate ion
33
34 (bond lengths 2.32 and 2.39 Å). As a consequence, pyridine ring orientation slightly deviates
35
36 from planarity ($\tau = 56.1$).
37
38
39

40
41 In the optimized structure of **2**, Ag ion has coordination number four with seesaw
42
43 geometry. Perchlorate ion is a bidentate ligand which forms two Ag-O coordination bonds with
44
45 bond lengths 2.56 Å. Ag-N coordination bonds are shorter (2.17 Å). Two *ortho* C-H bonds of
46
47 pyridine ligands form two C-H/O interactions with equal lengths (2.33 Å) with both ligating
48
49 atoms of perchlorate ion. These interactions are responsible for mutual orientation of pyridine
50
51 ligands, which is defined by dihedral angle between mean planes of these ligands ($\tau = 56.1^\circ$).
52
53
54
55
56
57
58
59
60
61
62
63
64
65

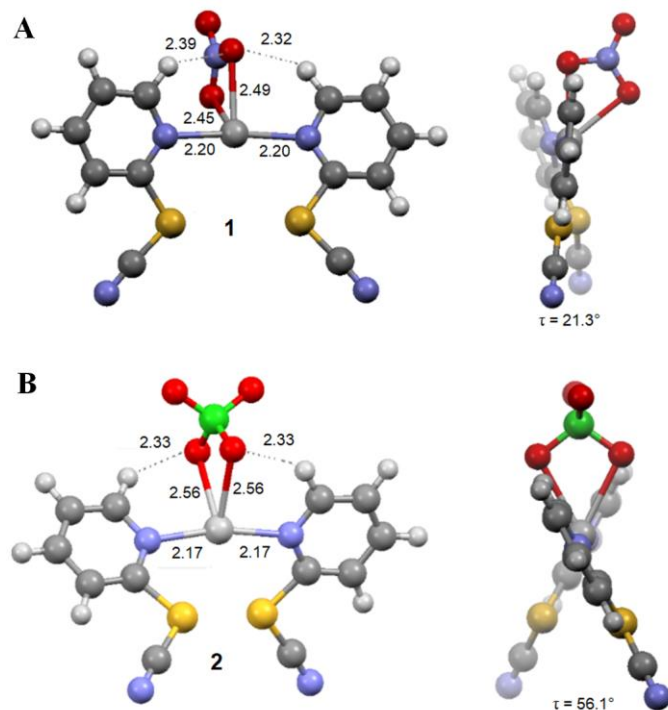
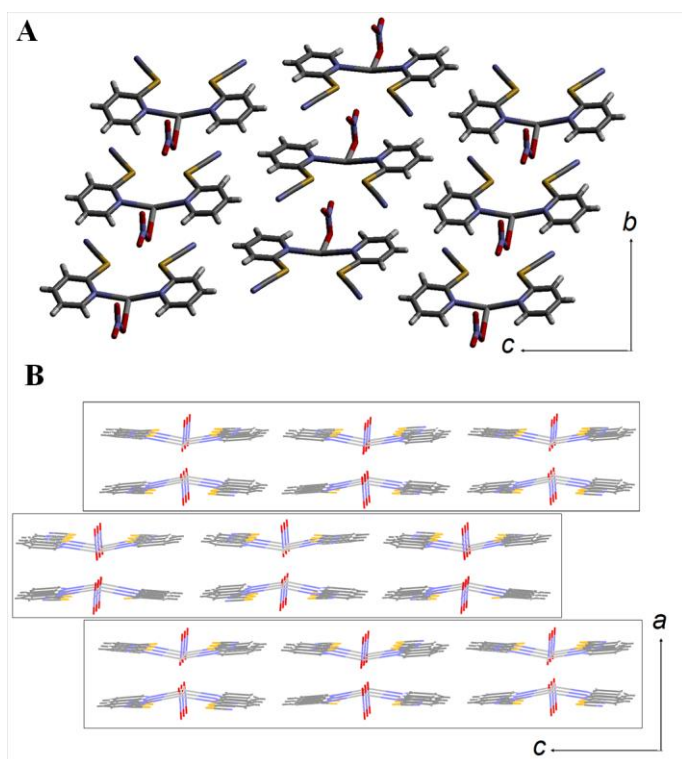


Figure 3. Optimized structures of **1** (A) and **2** (B).

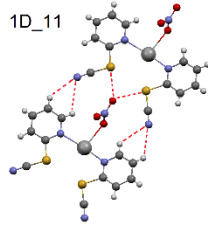
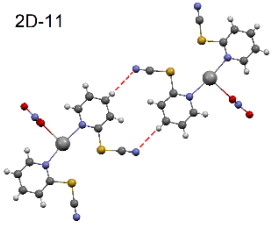
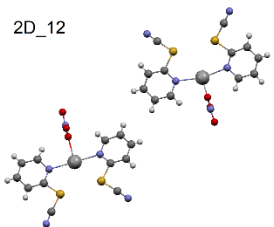
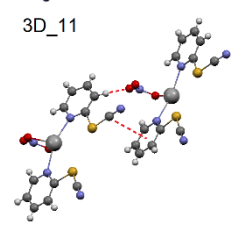
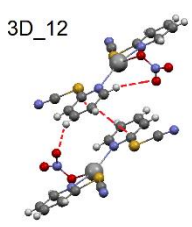
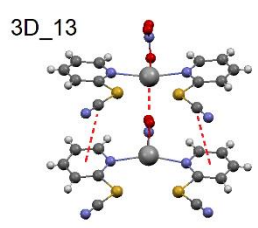
Energy of interactions of all orientations observed in the crystal structures of **1** and **2** are given in Tables 4 and 5, respectively. The structure of **1** can be described as packing of 1D chains formed along *b*-axis (Figure 4) resulting from interactions in 1D-11 orientation, into 2D layers in *bc* plane where two orientations (2D-11 and 2D-12) exist. The $-\text{SCN}$ group is involved in all three interactions observed in 1D-11 orientation. In the case of 2D orientation, 2D-11 orientation is based exclusively on $\text{C}-\text{H}\cdots\text{NCS}$ interactions while contribution of 2D-12 orientation is insignificant (-0.07 kcal/mol), which is expected for orientation with $\text{H}\cdots\text{H}$ contacts (Table 4). Layers are packed along *a*-axis (Figure 4), where every complex interacts with two complexes from one adjacent layer (3D-11 and 3D-12 orientations, Table 4), and one complex from another adjacent layer (3D-13 orientations, Table 4). Nitrate group is involved in

1
2
3
4 interactions in all three 3D orientations, among which 3D-13 orientation has two strongest
5
6 interaction energies above all six orientations in **1**. In this orientation both $-SCN$ groups from
7
8 one complex form π - π interactions with pyridine rings of another parallel complex. Parallel
9
10 interactions of pyridine rings also contribute to stabilization because aromatic ring interactions
11
12 have significant energy even with great offsets [32].
13
14
15
16
17
18

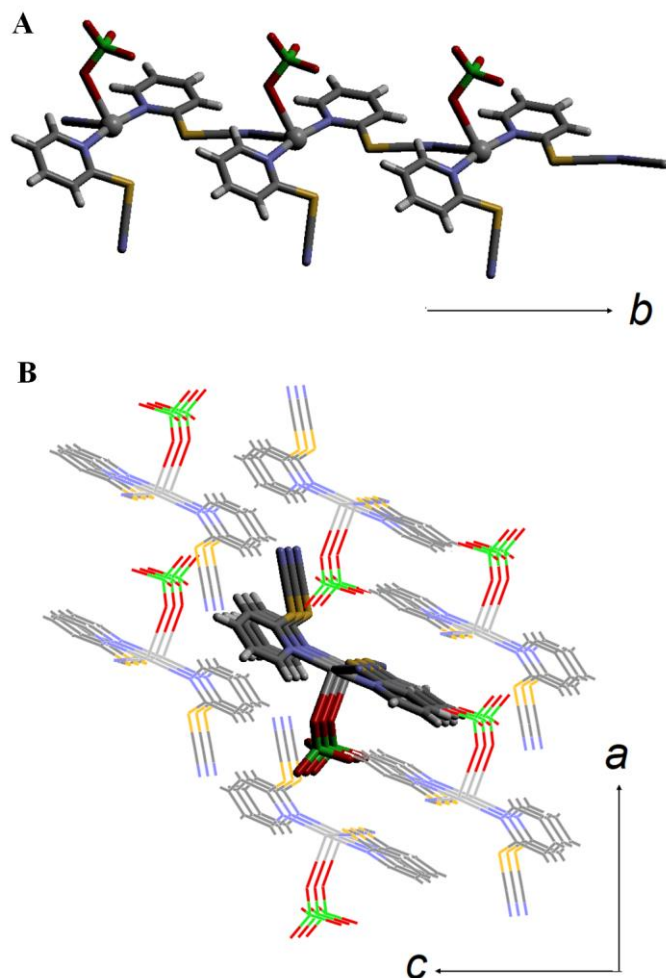


45 **Figure 4.** The packing in the crystal structure of **1**, illustrated by supramolecular structure within
46
47 the layer (A) and between layers (B).
48
49
50
51
52
53
54
55
56
57
58
59
60
61
62
63
64
65

Table 4. Illustrations of orientations, corresponding interactions and interaction energies (in kcal/mol), used to describe the packing in the crystal structure of **1**.

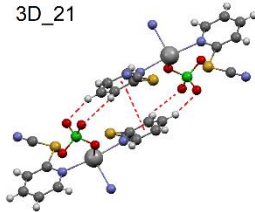
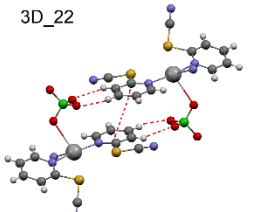
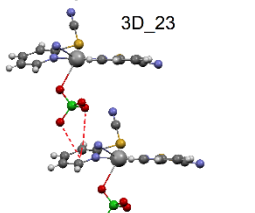
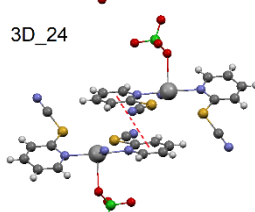
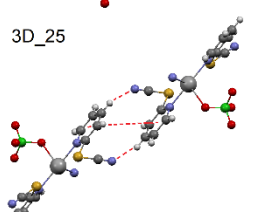
Orientation	Interactions	Interaction energy
 <p>1D_11</p>	<p>C–H···N_{SCN}</p> <p>O···S_{SCN}</p> <p>O···C_{SCN}</p>	–17.05
 <p>2D_11</p>	C–H···N _{SCN}	–4.03
 <p>2D_12</p>	H···H contacts	–0.07
 <p>3D_11</p>	<p>π-π (SCN···pyridine)</p> <p>C–H···O</p>	–10.59
 <p>3D_12</p>	<p>π-π (pyridine···pyridine)</p> <p>C–H···O</p>	–13.80
 <p>3D_13</p>	<p>π-π (SCN···pyridine)</p> <p>Ag···O</p>	–18.96

1
2
3
4 Contrary to **1**, complex **2** represent coordination polymer stretching along *b*-axis direction
5
6 in which Ag atom has coordination number four and *syn* geometry of perchlorate ion (Figure 5).
7
8 The polymeric chain interacts with six chains. Three adjacent chains are *syn*, while other three
9
10 are in *anti* position relative to perchlorate ion of the central polymeric chain.
11
12
13
14
15
16
17
18
19
20
21
22
23
24
25
26
27
28
29
30
31
32
33
34
35
36
37
38
39
40
41
42
43
44
45
46
47
48
49
50
51
52



53 **Figure 5.** The chain (A) and packing of chains (B) in the crystal structure of **2**.
54
55
56
57
58
59
60
61
62
63
64
65

Table 5. Illustration of orientations, corresponding interactions and interaction energies (in kcal/mol), used to describe the packing in the crystal structure of **2**.

Orientation	Interactions	Interaction energy
 <p>3D_21</p>	π - π (pyridine \cdots pyridine) C-H \cdots O	-22.41
 <p>3D_22</p>	π - π (pyridine \cdots pyridine) C-H \cdots O	-20.96
 <p>3D_23</p>	anion/ π (ClO ₄ ⁻ \cdots pyridine)	-11.23
 <p>3D_24</p>	π - π (pyridine \cdots pyridine)	-8.71
 <p>3D_25</p>	C-H \cdots N _{SCN} π - π (pyridine \cdots pyridine with great displacement)	-4.85

Syn oriented chains form interactions with the central chain, which could be described by orientations labeled as 3D-21, 3D-22, and 3D-23 (Table 5). There are stacking interactions between pyridine rings, accompanied by C-H/O interactions of pyridine C-H bonds with O

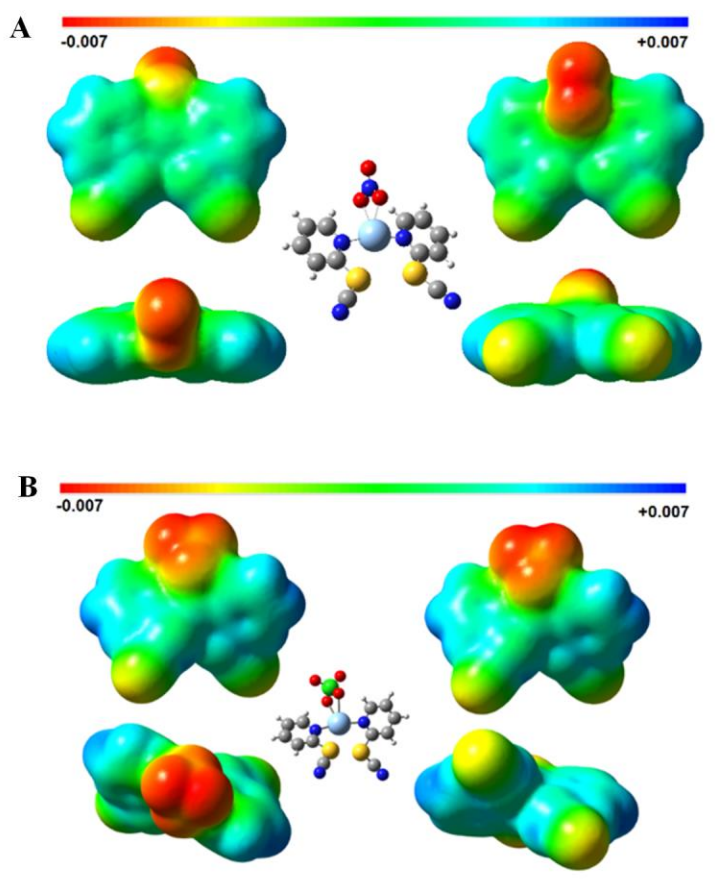
1
2
3
4 atoms of perchlorate ions (3D-21, 3D-22 orientations, Table 5). It is known that face to face
5
6 geometry of pyridine rings is weaker than displaced one [33]. That is the reason why 3D-22
7
8 orientation has lower bonding energy compared to 3D-21 orientation. In 3D-23 orientation
9
10 perchlorate ion interacts with π system of pyridine ring *via* anion/ π type interactions. This type of
11
12 non-covalent interactions is considered as weak non-covalent interactions. Several studies have
13
14 shown that the binding energies of non-covalent interactions between electron deficient aromatic
15
16 rings and anions are comparable to hydrogen bonds (from 4.5 to 12 kcal/mol) [34]. Although
17
18 these interactions are not typical for pyridine ring, we have shown that in the case of coordinated
19
20 pyridine it could be very strong (-11.23 kcal/mol).
21
22
23
24

25
26 Chains oriented *anti* relative to perchlorate ion also form π - π aromatic interactions of
27
28 pyridines with the central chain (3D-24 and 3D-25 orientations, Table 5), although in 3D-25
29
30 orientation the rings interact with greater displacement. This interaction is additionally stabilized
31
32 by C-H/N type interactions between pyridine rings and both -SCN groups. The parallel
33
34 interactions with great displacement are recently observed between benzene molecules [33]. It is
35
36 useful to point out that our calculations show that parallel-displaced orientations with
37
38 overlapping of coordinated pyridines are more stable than orientations without overlapping.
39
40
41
42

43
44 Based on analysis of packing in the crystal structure of **1**, one can conclude that C-H/O
45
46 interactions of pyridine rings are responsible for stabilization of the structure within the layers,
47
48 while their π - π stacking interactions are the most common among these layers (Table 4).
49
50 However, **2** does not form the layers, and in stabilization of the structure the π - π stacking
51
52 interactions of pyridine rings dominate (Table 5).
53
54

55
56 To understand the packing of investigated complexes in the crystal structures, maps of
57
58 electrostatic potentials for **1** and **2** fragments are made. On the maps (Figure 6), the potential
59
60
61
62
63
64
65

1
2
3
4 above non-coordinated O atoms are the most negative, while the potential above coordinated O
5
6 atoms and N atoms of SCN groups is slightly negative. Neutral potential is located above Ag and
7
8 atoms and N atoms of SCN groups is slightly negative. Neutral potential is located above Ag and
9
10 S–C bonds of SCN group, and partially above π -system of the pyridine rings. The remaining π -
11
12 system has a slightly positive potential, although the most positive potential is located above the
13
14 H atoms. Based on maps, the greatest contribution of electrostatic attraction should be expected
15
16 for interactions of pyridine C–H groups with O atoms (C–H/O interaction) and for C–H/N
17
18 interactions between C–H groups and N atoms of SCN groups. Significant contribution of
19
20 electrostatic attraction should also be expected in π - π interactions of SCN group with π -system
21
22 of pyridine ring.
23
24



56
57 **Figure 6.** Map of the electrostatic potential for **1** (A) and **2** (B).
58
59
60
61
62
63
64
65

Interactions of $-SCN$ group with a pyridine ring – CSD analysis

Based on the above mentioned it can be concluded that substitution of H atom with SCN group in aromatic systems significantly contributes to reinforcing π - π interactions. In order to determine the geometry of these interactions, a search of CSD was performed. The criteria we used for the search (Figure 7A) is that a distance between the center of pyridine ring (Cg) and the center of C \equiv N bond (Ω) is shorter than 4.0 Å, and angle β is less than 30° (the angle between Ω →Cg vector and the plane of pyridine ring). The search resulted in 60 crystal structures with 76 interactions (27 intermolecular and 49 intramolecular interactions). In most of them, the coordinated SCN groups participate in interactions (70 interactions, Figure 7B), while only 6 interactions have uncoordinated SCN group.

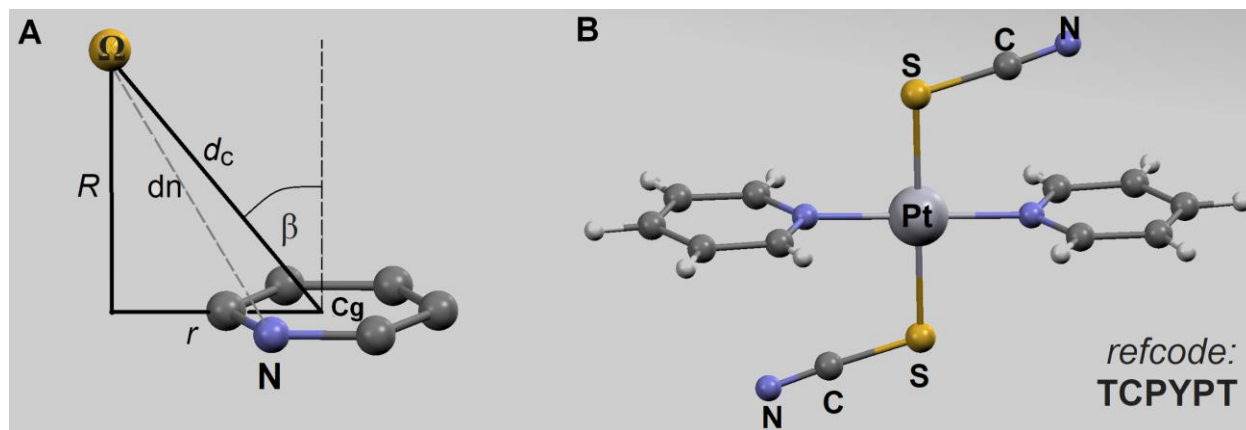


Figure 7. The illustrated criterion and geometric parameters used for a search of the CSD (A): the distance of the any atom from the center of the ring is denoted by d_c ; the distance of the ring center and the projection of an atom at the plane of the ring is the offset value (r); the normal distance of an atom from the plane of pyridine ring is denoted as R; and the distance of any atom from the N pyridine atom is denoted by dn. The fragment of crystal structure with refcode TCPYPT (B) with intramolecular interaction between SCN ligand and pyridine ring.

1
2
3
4 In order to analyse the offset values distribution, some offset values needed for a successful
5
6 distribution interpretation are introduced. The distance from the ring centre to the middle of C–C
7
8 or C–N bonds or to C and N atom of ring are found to be in the interval from 1.2 to 1.5 Å. Thus,
9
10 the atom with offset value less than 1.5 Å can be considered as atom above the ring or in the
11
12 immediate vicinity of the ring's edges. Since the distance from the centre to H atoms is around
13
14 2.4 Å, the interval from 1.5 to 2.4 Å was assigned as C–H bond region or the region just behind
15
16 N. The region above 2.4 Å was assigned as the region outside the ring. From the offset value
17
18 distributions (Figure 8A) one can conclude that N atoms have a tendency to be above the ring or
19
20 in the immediate vicinity of its edges, C atom have a tendency to be in the C–H bond region or in
21
22 the region close to N atoms, while S has a tendency for quite higher values, outside the ring
23
24 (tendency of certain atoms corresponds to the geometry shown in Figure 7B). In the case of
25
26 normal distances (R), the distributions show that S has a tendency for the lowest R values, while
27
28 N goes for the highest (Figure 8B). Thus, we can conclude that the SCN group is slightly tilted
29
30 with respect to the plane of the ring. This is also confirmed by the distribution of ΔR_{S-C} and
31
32 $\Delta R_{C=N}$ values (Figure 8C). The negative values of ΔR_{X-Y} indicate that atom X is closer to the
33
34 plane of the ring than atom Y. Also, higher value of ΔR_{X-Y} indicates greater deviation of atom X
35
36 from the parallel orientation. If we conditionally take values of this parameter in the interval
37
38 from –0.3 to 0.3 which corresponds to the parallel orientation, it is clear that the most common
39
40 orientations are with parallel orientation and mildly inclined orientation, but so that S is the
41
42 closest ring level, and N is the most distant. A slightly tilted orientation of SCN group and
43
44 pyridine ring is the result of simultaneous coordination of S atom from SCN group and pyridine
45
46 N atom to the same metal ion and the tetrahedral geometry of M–S–C domain (illustrated in
47
48 Figure 7B).
49
50
51
52
53
54
55
56
57
58
59
60
61
62
63
64
65

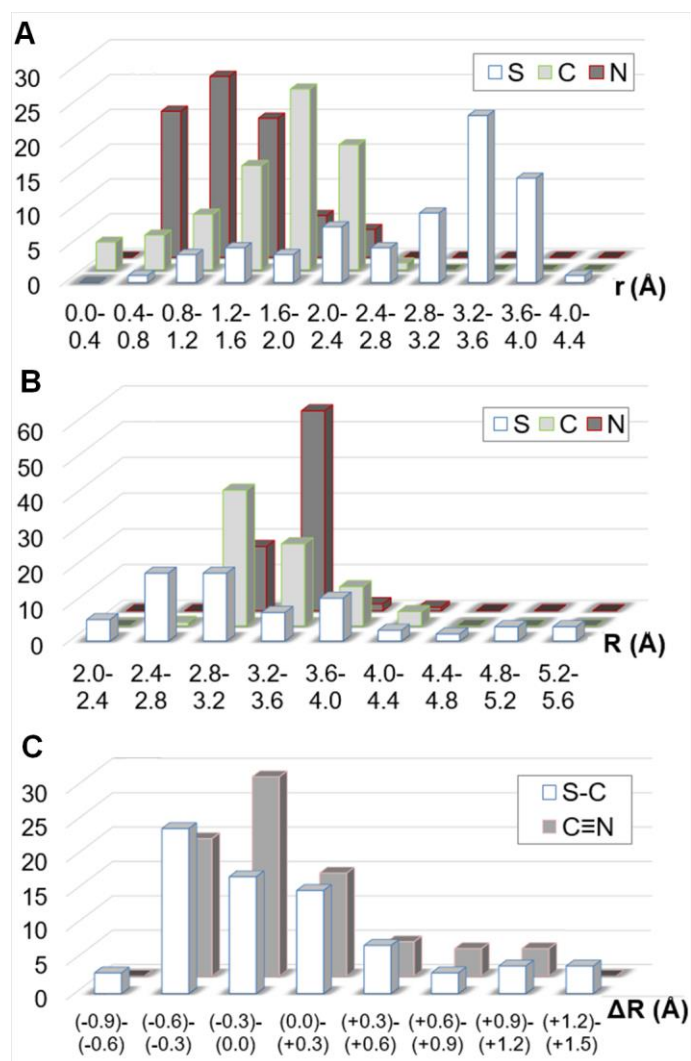


Figure 8. Distribution of offset values (A) and normal distances (B) for S, C, and N atoms of SCN group, and distribution of ΔR parameter (C) for S–C bond ($\Delta R_{S-C} = R_S - R_C$) and for C \equiv N bond ($\Delta R_{C\equiv N} = R_S - R_N$) of SCN group.

Parameter Δd_x ($\Delta d = d_n - d_c$), for X = S, C, and N atom of SCN group are used to estimate the orientation of the atom relative to ring center and to pyridine N atom (Δd_S , Δd_C , and Δd_N parameters, Figure 9A). Positive value of the parameter indicates that atom is closer to the N

atom than the center of ring. It is clear that all three atoms are mainly in positions close to the N atom rather than the center of the ring, while S atom has the maximum of Δd distribution at the highest positive values, indicating that the S atom tends to be the closest to pyridine N atom, compared to other two atoms of SCN group. The torsion angle T describes the orientation of the $C\equiv N$ group and the vector starting from the N atom to the center of pyridine ring ($N-Cg\cdots C\equiv N$ torsion angle). The maximum that appears on the distribution graph (close to 180°) corresponds to the anti-orientation (Figure 9B).

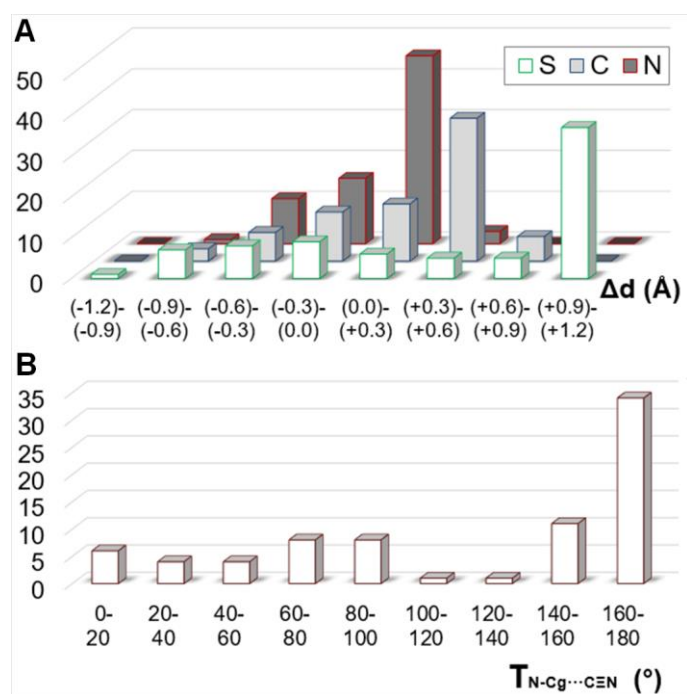


Figure 9. Distribution of Δd values for S, C, and N atom of SCN group (A) and torsion angle $T(N-Cg\cdots C\equiv N)$ values (B).

If we take all these distributions into consideration, the geometry of the SCN group can be displayed by the orientation found in the structure with the TCPYPT refcode (Figure 7B).

1
2
3
4 Such trends are the result of a large number of structures in which intramolecular interaction
5
6 occurs between coordinated SCN group and coordinated pyridine. The interactions of
7
8 uncoordinated SCN group with pyridine ring have no tendency towards some value of the torsion
9
10 angle T. It is similar with both offset and Δd values. There is only the tendency toward the
11
12 parallel orientations. The similar propensity is established in our crystal structures, in which the
13
14 SCN group has a role of pyridine substituent. In 3D-11 and 3D-13 orientations of **1** (Table 4), the
15
16 C \equiv N group is located above the pyridine ring, with almost parallel alignment and torsional
17
18 angles T which do not correspond to anti-orientation ($T_{3D-11} = 51.7^\circ$ and $T_{3D-13} = 126.1^\circ$). In the
19
20 crystal structure of **2**, the pyridine rings are overlapping with other ones rather than with SCN
21
22 substituents. Differences in the mutual orientation of SCN substituent and pyridine ring,
23
24 established in these crystal structures, can be explained by the differences in metal complex
25
26 geometries.
27
28
29
30
31
32
33
34
35

36 *Antiproliferative activity*

37
38 The antiproliferative activity of monomeric compound **1** and L was studied in a panel of
39
40 representative human solid tumor cell lines. Polymeric complex **2** was not soluble enough to be
41
42 tested. The results expressed as GI₅₀ values in μM are given in Table 6. Overall, the GI₅₀ values
43
44 in all cell lines were in the low micromolar range. Importantly, in resistant cell lines T-47D and
45
46 WiDr, the activity of **1** was significantly higher than the standard anticancer drugs cisplatin and
47
48 5-FU.
49
50
51
52
53
54
55
56
57
58
59
60
61
62
63
64
65

Table 6. Antiproliferative activity of tested substances

Compound	GI ₅₀ (μM)			
	HBL-100	HeLa	T-47D	WiDr
L	15 ± 5	19 ± 8	29 ± 7	37 ± 2
1	2.3 ± 0.3	2.4 ± 0.7	2.8 ± 0.7	4.2 ± 0.5
cisplatin	1.9 ± 0.2	2.0 ± 0.3	15 ± 2.3	26 ± 6
5-FU	5.5 ± 2.3	15 ± 5	47 ± 18	49 ± 7
AgNO ₃	15 ± 4	16 ± 1	19 ± 2	13 ± 2

Docking studies on DNA and HSA

Cellular DNA represents a major pharmacological target of the majority of metal-based drugs [35]. On the other hand, HSA is ligand binder which stores wide range of molecules making it an important factor in pharmacokinetic behavior of anticancer drugs candidates [36]. In this study, we used molecular docking, as an extremely useful tool in drug discovery, for studies of drug/biomolecule interactions [37], to investigate DNA as possible target for **1**, and HSA as its possible carrier to blood stream.

Docking results to DNA (pdf code 1BNA, Figure 10) showed that **1** has propensity to bind in DNA minor groove. There are three conformers bind in major groove. Three types of ligand binding to DNA are known: intercalation of ligand between adjacent base pairs, ligand binding in the minor groove and binding in the major groove. Small molecules are binding substantially in the minor groove or they intercalate [38–40], although the intercalation is

1
2
3
4 sequentially demanding and requires a GC-rich region [38,40,41]. The majority of drugs that
5
6 bind in the minor groove have a tendency toward AT-rich region [39,42–44].
7
8

9 Complex **1** shows higher tendency for binding in GC-rich regions (–5.14 kcal/mol) than
10
11 to AT-rich region (–4.68 kcal/mol). The binding for AT region is also conformationally
12
13 unfavorable. Complex **1** possesses higher conformational freedom for binding in GC-rich region
14
15 (31 conformers) than to AT-rich region (8 conformers). As previously mentioned, it is
16
17 reasonable to achieve that **1** will intercalate in DNA, which is in accord to visual analysis of
18
19 DNA crystal structures archived in Protein Data Base (PDB). Namely, the metal complexes with
20
21 aromatic ligands in PDB are mainly intercalated between DNA bases.
22
23
24

25
26 Beside intercalation, there is a big probability that certain quantity of **1** will be bonded in
27
28 minor groove, between GC and AT-rich region. Docking results showed that the binding in this
29
30 region is energetically (–5.22 kcal/mol) and conformationally favorable (57 conformers), in
31
32 comparison with two previously described binding regions.
33
34
35
36
37
38
39
40
41
42
43
44
45
46
47
48
49
50
51
52
53
54
55
56
57
58
59
60
61
62
63
64
65

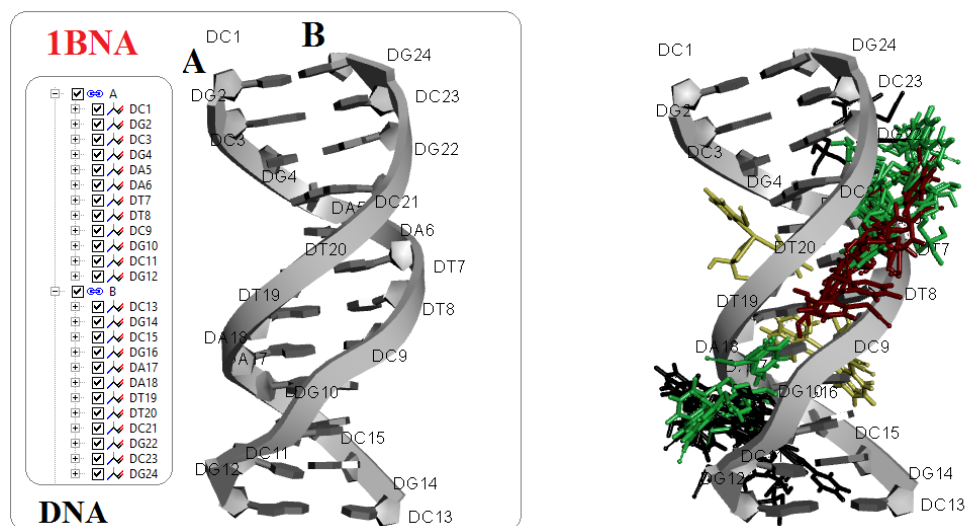
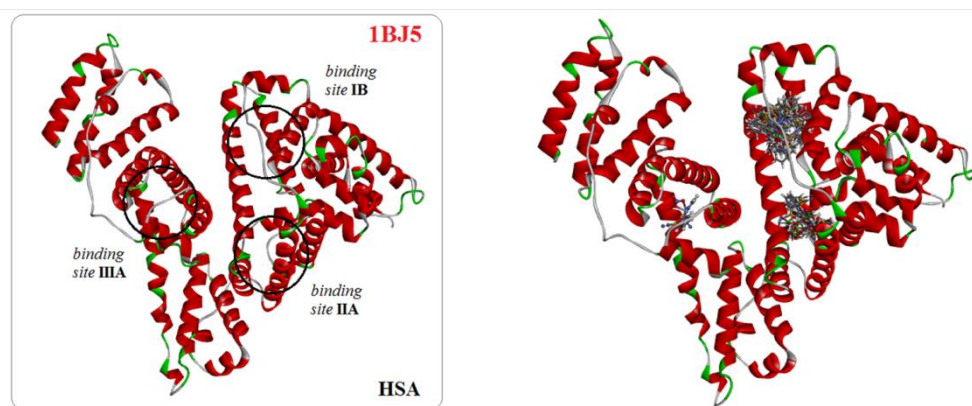


Figure 10. Structure of DNA with labeled sequence (left) together with binding clusters of **1** (right). Black colored complexes bind in GC-rich region of minor groove, red complexes bind in AT-rich region of minor groove, while green complexes bind at minor groove between GC- and AT-rich regions. Yellow complexes bind into major groove.

The docking study for binding of **1** (corresponding to the main synthons, used to explain the packaging in crystal structures) at HSA (PDB code 1BJ5) showed that **1** forms three binding clusters, at I_B, II_A and III_A subdomains of HSA (Figure 11), with binding energies greater than -5.0 kcal/mol. Complex **1** has the tendency for binding at site in I_B subdomain with binding energy of -6.70 kcal/mol, and 38 conformers of **1** with HSA. The second binding site is located in III_A subdomain, with binding energy of -6.10 kcal/mol, and 3 conformers of **1** with HSA. The binding in the third binding site, located in II_A subdomain, has significantly lower energy (-5.74 kcal/mol), but much higher conformational freedom (35 conformers of **1** with HSA), compared to second binding site.

1
2
3
4 By visual analysis of crystal structures of HSA, we concluded that the fatty acids, which
5 are often accompanied the HSA, is also capable to bind at all three binding sites. Therefore, the
6 binding of **1** is competitive to binding of fatty acids. However, analysis of crystal structures of
7 HSA from PDB has shown that the aromatic compounds commonly bounded to all three binding
8 sites in HSA, which leads us to conclude that **1** could bind to these binding sites and transported
9 in the blood.
10
11
12
13
14
15
16
17
18



19
20
21
22
23
24
25
26
27
28
29
30
31
32
33
34 **Figure 11.** Structure of human serum albumin (HSA) with labeled binding sites (left) and
35 together with binding clusters of **1** (right).
36
37
38
39
40

41 **Conclusions**

42
43
44 Unprecedented silver based-complexes with 2-pyridylthiocyanate ligand were
45 synthesized and characterized by a single crystal XRD analysis. Molecular structure of nitrate
46 based complex **1** consists of monodentately coordinated two L molecules *via* pyridine nitrogen
47 atoms, while third coordination site is occupied by oxygen atom from nitrate ion. Close
48 inspection of coordination sphere around Ag(I) revealed additional weak interaction(s) of central
49 metal ion with oxygen atoms of nitrate ion. However, QTAIM analysis revealed that all Ag \cdots O
50 interactions have ionic nature, while the shortest interaction can be treated as a bond because of
51
52
53
54
55
56
57
58
59
60
61
62
63
64
65

1
2
3
4 its partial covalent character. This is also supported by a CSD analysis where the shortest Ag(I)–
5
6 O interaction in **1** is in the range corresponding to maximum for distribution of bond distance
7
8 parameter. Perchlorate-based compound **2** represents 1D coordination polymer since thiocyanate
9
10 nitrogen atom from third L molecule is coordinated to Ag(I), besides two pyridine nitrogen
11
12 atoms. Although XRD analysis showed that perchlorate ion is coordinated to Ag(I) in **2**, QTAIM
13
14 topological analysis showed that this anion provides less electron density to Ag(I) in comparison
15
16 to nitrate, thus enabling bis-monodentate coordination of each L ligand. The consequence of this
17
18 is extension of structure to infinite 1D chain. Analyzed structures with the same organic
19
20 thiocyanate ligand represent an example where the nature of (non)coordinated ions were found to
21
22 have the profound influence on coordination mode of the ligand and consequently packing in the
23
24 crystal structure.
25
26
27
28
29

30
31 Study of energy distribution of intermolecular interactions in crystal structures of **1** and **2**,
32
33 explained the differences in packing between these compounds. In the crystal structure of **1**
34
35 C–H/O interactions of pyridine rings are responsible for stabilization of the structure within the
36
37 layers, while their π - π stacking interactions are the most common among these layers. However,
38
39 **2** does not form the layers, and crystal packing is dominated by π - π stacking interactions of
40
41 pyridine rings. Obtained results are in accord with the maps of electrostatic potentials for both
42
43 structures.
44
45
46
47

48 The results of antiproliferative activity indicate that coordination of the ligand to silver is
49
50 crucial, since metal-free ligand and starting silver salt used in synthesis did not show significant
51
52 activity. Remarkably, complex **1** showed comparable or even better antiproliferative activity than
53
54 cisplatin and 5-FU in all tested human solid tumor cell lines. With the aid of docking study it was
55
56 shown that **1** could intercalate to DNA and could be transported to blood stream *via* HSA.
57
58
59
60
61
62
63
64
65

1
2
3
4 Although this is the first study on antiproliferative activity of **1**, current results strongly approve
5
6 its further testing onto other cancer models and elucidation of its mechanism of action.
7
8
9

10 11 **Electronic Supplementary Information**

12
13 Crystallographic structural data have been deposited at the Cambridge Crystallographic Data
14
15 Centre (CCDC). Enquiries for data can be direct to: Cambridge Crystallographic Data Centre, 12
16
17 Union Road, Cambridge, UK, CB2 1EZ or (e-mail) deposit@ccdc.cam.ac.uk or
18
19 (fax) +44 (0) 1223 336033. Any request to the Cambridge Crystallographic Data Centre for this
20
21 material should quote the full literature citation and the reference numbers CCDC 1916786 for
22
23 complex **1** and 1916787 for complex **2**.
24
25
26
27
28
29
30

31 **Conflicts of Interest**

32
33 There are no conflicts of interest to declare.
34
35
36
37

38 **Acknowledgments**

39
40 The Ministry of Education, Science and Technological Development of the Republic of Serbia
41
42 under Grant 172057 supported this work. The CNRS and the University of Strasbourg are
43
44 acknowledged for their recurrent funding support. AP and JMP thank the Spanish Government
45
46 for financial support through project PGC2018-094503-B-C22 (MCIU/AEI/FEDER, UE).
47
48
49
50
51
52
53
54
55
56
57
58
59
60
61
62
63
64
65

References

- [1] C. R. Groom, I. J. Bruno, M. P. Lightfoot and S. C. Ward, *Acta Crystallogr. Sect. B Struct. Sci. Cryst. Eng. Mater.*, **72**, 2016, 171–179.
- [2] T. Castanheiro, J. Suffert, M. Donnard and M. Gulea, *Chem. Soc. Rev.*, **45**, 2016, 494–505.
- [3] H. Martínez-García, D. Morales, J. Pérez, M. Puerto and D. Miguel, *Inorg. Chem.*, **49**, 2010, 6974–6985.
- [4] R. K. Prajapati and S. Verma, *Inorg. Chem.*, **50**, 2011, 3180–3182.
- [5] C. N. Banti and S. K. Hadjikakou, *Metallomics*, **5**, 2013, 569.
- [6] Z. Engelbrecht, R. Meijboom and M. J. Cronjé, *BioMetals*, **31**, 2018, 189–202.
- [7] C.-Y. Su, C.-L. Chen, J.-Y. Zhang and B.-S. Kang, in *Design and Construction of Coordination Polymers*, John Wiley & Sons, Inc., Hoboken, NJ, USA, 2009, pp. 111–144.
- [8] T. Castanheiro, M. Gulea, M. Donnard and J. Suffert, *Eur. J. Org. Chem.*, **2014**, 2014, 7814–7817.
- [9] Oxford Diffraction (2006). CrysAlis CCD and CrysAlis RED. Oxford Diffraction Ltd, Abingdon, Oxfordshire, England.
- [10] Bruker (2012). Bruker APEX2. Bruker AXS Inc., Madison, Wisconsin, USA.
- [11] R. H. Blessing and IUCr, *Acta Crystallogr. Sect. A Found. Crystallogr.*, **51**, 1995, 33–38.
- [12] G. M. Sheldrick, *Acta Crystallogr. Sect. C Struct. Chem.*, **71**, 2015, 3–8.
- [13] A. L. Spek, *J. Appl. Crystallogr.*, **36**, 2003, 7–13.
- [14] L. J. Farrugia, *J. Appl. Crystallogr.*, **32**, 1999, 837–838.
- [15] C. F. Macrae, I. J. Bruno, J. A. Chisholm, P. R. Edgington, P. McCabe, E. Pidcock, L.

- 1
2
3
4 Rodriguez-Monge, R. Taylor, J. van de Streek and P. A. Wood, *J. Appl. Crystallogr.*, **41**,
5
6 2008, 466–470.
7
8
- [16] Gaussian 09, Revision A.02, M. J. Frisch, G. W. Trucks, H. B. Schlegel, G. E. Scuseria,
9
10 M. A. Robb, J. R. Cheeseman, G. Scalmani, V. Barone, G. A. Petersson, H. Nakatsuji, X.
11
12 Li, M. Caricato, A. Marenich, J. Bloino, B. G. Janesko, R. Gomperts, B. Mennucci, H. P.
13
14 Hratchian, J. V. Ortiz, A. F. Izmaylov, J. L. Sonnenberg, D. Williams-Young, F. Ding, F.
15
16 Lipparini, F. Egidi, J. Goings, B. Peng, A. Petrone, T. Henderson, D. Ranasinghe, V. G.
17
18 Zakrzewski, J. Gao, N. Rega, G. Zheng, W. Liang, M. Hada, M. Ehara, K. Toyota, R.
19
20 Fukuda, J. Hasegawa, M. Ishida, T. Nakajima, Y. Honda, O. Kitao, H. Nakai, T. Vreven,
21
22 K. Throssell, J. A. Montgomery, Jr., J. E. Peralta, F. Ogliaro, M. Bearpark, J. J. Heyd, E.
23
24 Brothers, K. N. Kudin, V. N. Staroverov, T. Keith, R. Kobayashi, J. Normand, K.
25
26 Raghavachari, A. Rendell, J. C. Burant, S. S. Iyengar, J. Tomasi, M. Cossi, J. M. Millam,
27
28 M. Klene, C. Adamo, R. Cammi, J. W. Ochterski, R. L. Martin, K. Morokuma, O. Farkas,
29
30 J. B. Foresman, and D. J. Fox, Gaussian, Inc., Wallingford CT, 2009.
31
32
- [17] F. W. Biegler-König, R. F. W. Bader and T.-H. Tang, *J. Comput. Chem.*, **3**, 1982, 317–
33
34 328.
35
36
- [18] T. Lu and F. Chen, *J. Comput. Chem.*, **33**, 2012, 580–592.
37
38
- [19] T. A. Keith, AIMAll (Version 13.10.19, <http://aim.tkgristmill.com>), T. G. S. Todd and A.
39
40 Keith, Overland Park KS, USA.
41
42
- [20] J. Contreras-García, E. R. Johnson, S. Keinan, R. Chaudret, J.-P. Piquemal, D. N. Beratan
43
44 and W. Yang, *J. Chem. Theory Comput.*, **7**, 2011, 625–632.
45
46
- [21] C. I. Bayly, P. Cieplak, W. Cornell and P. A. Kollman, *J. Phys. Chem.*, **97**, 1993, 10269–
47
48 10280.
49
50
51
52
53
54
55
56
57
58
59
60
61
62
63
64
65

- 1
2
3
4 [22] H. R. Drew, R. M. Wing, T. Takano, C. Broka, S. Tanaka, K. Itakura and R. E. Dickerson,
5
6 *Proc. Natl. Acad. Sci. U. S. A.*, **78**, 1981, 2179–83.
7
8
9 [23] S. Curry, H. Mandelkow, P. Brick and N. Franks, *Nat. Struct. Biol.*, **5**, 1998, 827–835.
10
11 [24] G. M. Morris, R. Huey, W. Lindstrom, M. F. Sanner, R. K. Belew, D. S. Goodsell and A.
12
13 J. Olson, *J. Comput. Chem.*, **30**, 2009, 2785–91.
14
15
16 [25] Dassault Systèmes BIOVIA, Discovery Studio Modeling Environment (Release 2017),
17
18 San Diego, Dassault Systèmes, 2016.
19
20
21 [26] F. H. Allen, *Acta Crystallogr. Sect. B*, **58**, 2002, 380–388.
22
23
24 [27] I. J. Bruno, J. C. Cole, P. R. Edgington, M. Kessler, C. F. Macrae, P. McCabe, J. Pearson
25
26 and R. Taylor, *Acta Crystallogr. Sect. B Struct. Sci.*, **58**, 2002, 389–397.
27
28
29 [28] H. Elshafly, T. R. Todorović, M. Nikolić, A. Lolić, A. Višnjevac, S. Hagenow, J. M.
30
31 Padrón, A. T. García-Sosa, I. S. Djordjević, S. Grubišić, H. Stark and N. R. Filipović,
32
33 *Front. Chem.*, **6**, 2018, 247.
34
35
36 [29] E. Pretsch, P. Bühlmann and M. Badertscher, in *Structure Determination of Organic*
37
38 *Compounds*, Springer Berlin Heidelberg, Berlin, Heidelberg, 2009, pp. 1–67.
39
40
41 [30] K. Nakamoto, *Infrared and Raman Spectra of Inorganic and Coordination Compounds*,
42
43 John Wiley & Sons, Inc., Hoboken, NJ, USA, 2008.
44
45
46 [31] Bruker, 269-0159xx, SHELXTL Software reference manual, Bruker AXS Inc, 1997.
47
48 [32] D. B. Ninković, G. V. Janjić, D. Ž. Veljković, D. N. Sredojević and S. D. Zarić,
49
50 *ChemPhysChem*, **12**, 2011, 3511–3514.
51
52
53 [33] D. B. Ninković, G. V. Janjić and S. D. Zarić, *Cryst. Growth Des.*, **12**, 2012, 1060–1063.
54
55
56 [34] B. L. Schottel, H. T. Chifotides and K. R. Dunbar, *Chem. Soc. Rev.*, **37**, 2008, 68–83.
57
58 [35] L. S. Foteeva, M. Matczuk and A. R. Timerbaev, *TrAC - Trends Anal. Chem.*, **90**, 2017,
59
60
61
62
63
64
65

- 1
2
3
4 107–113.
5
6
7 [36] A. Božić, A. Marinković, S. Bjelogrić, T. R. Todorović, I. N. Cvijetić, I. Novaković, C.
8
9 D. Muller and N. R. Filipović, *RSC Adv.*, **6**, 2016, 104763–104781.
10
11 [37] N. R. N. R. Filipović, S. Bjelogrić, G. Portalone, S. Pelliccia, R. Silvestri, O. Klisurić, M.
12
13 Senćanski, D. Stanković, T. R. Todorović and C. D. Muller, *Medchemcomm*, **7**, 2016,
14
15 1604–1616.
16
17
18 [38] X. Han and X. Gao, *Curr. Med. Chem.*, **8**, 2001, 551–581.
19
20
21 [39] S. Neidle and C. M. Nunn, *Nat. Prod. Rep.*, **15**, 1998, 1–15.
22
23
24 [40] G. Bischoff and S. Hoffmann, *Curr. Med. Chem.*, **9**, 2002, 321–348.
25
26 [41] J. N. Lisgarten, M. Coll, J. Portugal, C. W. Wright and J. Aymami, *Nat. Struct. Biol.*, **9**,
27
28 2002, 57–60.
29
30
31 [42] S. Neidle, *Nat. Prod. Rep.*, **18**, 2001, 291–309.
32
33
34 [43] D. E. Wemmer, *Annu. Rev. Biophys. Biomol. Struct.*, **29**, 2000, 439–461.
35
36 [44] J. Ren and J. B. Chaires, *Biochemistry*, **38**, 1999, 16067–16075.
37
38
39
40
41
42
43
44
45
46
47
48
49
50
51
52
53
54
55
56
57
58
59
60
61
62
63
64
65

